

# Simultaneous magneto-optical trapping of lithium and ytterbium atoms towards production of ultracold polar molecules

M. Okano<sup>1</sup>, H. Hara<sup>1</sup>, M. Muramatsu<sup>1</sup>, K. Doi<sup>1</sup>, S. Uetake<sup>1,2</sup>, Y. Takasu<sup>1</sup>, Y. Takahashi<sup>1,2</sup>

<sup>1</sup> Department of Physics, Graduate School of Science, Kyoto University, Kyoto, Japan

<sup>2</sup> CREST, Japan Science and Technology Agency, Kawaguchi, Saitama, Japan

Received: date / Revised version: date

**Abstract** We have successfully implemented the first simultaneous magneto-optical trapping (MOT) of lithium (<sup>6</sup>Li) and ytterbium (<sup>174</sup>Yb) atoms, towards production of ultracold polar molecules of LiYb. For this purpose, we developed the dual atomic oven which contains both atomic species as an atom source and successfully observed the spectra of the Li and Yb atoms in the atomic beams from the dual atomic oven. We constructed the vacuum chamber including the glass cell with the windows made of zinc selenium (ZnSe) for the CO<sub>2</sub> lasers, which are the useful light sources of optical trapping for evaporative and sympathetic cooling. Typical atom numbers and temperatures in the compressed MOT are  $7 \times 10^3$  atoms, 640  $\mu$ K for <sup>6</sup>Li,  $7 \times 10^4$  atoms and 60  $\mu$ K for <sup>174</sup>Yb, respectively.

## 1 Introduction

Researches of ultracold gases of atoms have revealed the nature of the quantum degenerate gases since the first realization of the Bose-Einstein condensates (BEC) [1, 2] and the Fermi degenerates (FD) [3] of atoms. As a next important step, an ultracold gas of molecules has recently attracted much attention due to their unique properties and prospects for many applications [4]. In particular, molecules consist of two atomic species with different mass may have large electric dipole moments, called polar molecules. Electric dipole-dipole interactions of polar molecules are anisotropic and in a long-range, different from the contact interactions of atoms. In addition, dipole-dipole interactions of electric dipole moments are considered to be much stronger than those of magnetic dipole moments of atoms. Due to these strong long-range anisotropic interactions, many applications of

polar molecules have been theoretically proposed [5]. Polar molecules in optical lattices have particularly been worthy of attention for their applications including a quantum computation [6], the study of the frustrated states in the triangular lattices [7] and the quantum simulator of lattice-spin models [8].

Among the various combinations of atomic species, we have focused on ultracold gases of molecules composed of Li and Yb [9]. The molecule has the largest mass ratio ( $\sim 29$ ) among the combinations of atomic species that have already been cooled to quantum degenerate regime. The most important advantage of molecules of LiYb is the existence of a spin degree of freedom in the electronic ground molecular state ( $^2\Sigma$ ), which enables us to implement the quantum simulator of lattice-spin models. In contrast, molecules composed of alkali atoms in the singlet electronic ground molecular state ( $^1\Sigma$ ) have no electron spin degree of freedom. RbYb molecules, as well as LiYb molecules, have a spin degree of freedom in the  $^2\Sigma$  state and have recently been studied [10]. However, LiYb molecules have further advantages: (i) Li and Yb have both bosonic and fermionic isotopes and this leads to the study of various molecules composed of fermionic-fermionic, fermionic-bosonic and bosonic-bosonic atoms. In contrast, Rb has only bosonic isotopes. (ii) Due to their large mass ratio, weakly bound LiYb molecules of both fermionic isotopes are expected to be collisionally stable and promising for the study of the three-body system such as Efimov trimer states [11].

The expected processes for generating ultracold molecules of LiYb are as follows: First, Li and Yb atomic beams from an atomic oven are decelerated by the Zeeman slowing method and these cooled atoms are loaded to a magneto-optical trap (MOT) in a main chamber. Second, these trapped atoms are transferred to an optical trap and evaporatively cooled with sympathetic cooling of atoms between different atomic species [12]. Third, evaporatively cooled Li and Yb atoms are adiabatically associated to weakly bound LiYb molecules by employing magnetically tunable Feshbach resonances [13]. Fi-

nally, weakly bound molecules are coherently transferred to the rovibrational ground state of the electronic ground molecular state by employing a step of STIRAP (STImulated Raman Adiabatic Passage) [14].

In this paper, we report the first simultaneous MOT of Li and Yb atoms, towards production of ultracold polar molecules of LiYb. For this purpose, we developed the dual atomic oven which contains both atomic species and successfully observed the spectra of Li and Yb atomic beams from the dual atomic oven as described in Sect. 2. The laser systems and a glass cell as a main chamber are described in Sect. 3. In particular, the windows made of zinc selenium (ZnSe) are attached to the glass cell for the CO<sub>2</sub> laser, which is a useful light source of optical trapping for evaporative and sympathetic cooling as well as trapping of cold LiYb molecules. The procedures and experimental parameters of the simultaneous MOT of <sup>6</sup>Li and <sup>174</sup>Yb are discussed in Sect. 4.

## 2 Dual atomic oven

### 2.1 Atomic oven

We first developed the dual atomic oven which contains both Li and Yb atoms as an atom source. Developing the dual atomic oven is important to make experimental systems simple and compact. While temperatures of Li and Yb atoms are equal in the dual atomic oven, the saturated vapor pressure of Yb is at most an order of magnitude larger than that of Li at around 400 °C. The configuration of the dual atomic oven is shown in the left side of Fig. 1. This oven consists of three parts: the body part which contains Li and Yb atoms, the curved part and the nozzle part where atoms pass out through as the atomic beams. We designed the body part vertical because it is heated above the melting point of Li (180 °C). Approximately 60 thin tubes, each of which has a inner diameter of 0.3 mm and a length of 10 mm, are assembled at the nozzle part, which limits the divergence of the atomic beams by approximately 0.03 rad.

### 2.2 Spectroscopy using the atomic beams

One may expect that atoms could not pass out as the atomic beams because of reactions between Li and Yb in the atomic oven. To check the performance of the dual atomic oven, we employed the spectroscopy of Li and Yb atomic beams from the dual atomic oven. The light source for the Li spectroscopy is an extended cavity laser diode (ECLD) in the Littman configuration with a wavelength of 671 nm. For the Yb spectroscopy we also used an ECLD in the Littrow configuration with a wavelength of 399 nm. The Li and Yb metals with natural abundances were put in the body part of the atomic oven, which was heated to 460 °C by wires wound around. The vapor pressures of Li and Yb at this temperature

are  $1 \times 10^{-3}$  Torr and  $7 \times 10^{-3}$  Torr, respectively. The output laser beams of ECLDs with their laser frequencies tuned to  $2s$ - $2p$  transitions of Li and  $(6s^2) ^1S_0$ - $(6s6p) ^1P_1$  transitions of Yb were applied perpendicular to the atomic beams and fluorescences from the atomic beams were detected by a photo multiplier tube (PMT).

In this way we observed the spectra of Li and Yb atomic beams by measuring the fluorescence as shown in Fig. 2. The fluorescence signals of the  $D_2$  line of <sup>6</sup>Li and the  $D_1$  line of <sup>7</sup>Li in Fig. 2(a) were obtained with 16 times integration and those of  $^1S_0$ - $^1P_1$  transitions of Yb isotopes were also obtained (Fig. 2(b)). The Doppler widths of the fluorescence signals resulted from the angular divergence of the atomic beams are consistent with the configuration of the thin tubes at the nozzle part of the dual atomic oven. Thus the performance of the dual atomic oven was properly checked and the dual atomic oven was prepared for the experiment. The relative intensities of the each lines are consistent with the expectation [15].

## 3 Experimental setup

### 3.1 Laser systems

Energy levels and transitions for laser cooling and probing of <sup>6</sup>Li and <sup>174</sup>Yb atoms are shown in Fig. 3. We use transitions of the  $D_2$  line of <sup>6</sup>Li atoms for laser cooling and probing. The wavelength and the natural linewidth ( $\Gamma$ ) of the  $D_2$  line are 671 nm and  $2\pi \times 5.9$  MHz, respectively. As a light source we used a cw ring dye laser (Coherent, 899-21) with LD688 dye pumped by a cw green diode-pumped solid-state laser (Coherent, Verdi-V8) with a wavelength of 532 nm and a power of 6 W. The output power of the cw ring dye laser is 400 mW. The output beam of the dye laser is divided into laser beams for MOT, MOT repumping, Zeeman slowing, probe, probe repumping, and frequency locking of the dye laser. The use of repumping beams (MOT repumping beam and probe repumping beam) is essentially important because the hyperfine splittings of the excited state ( $^2P_{3/2}$ ) are comparable with the natural linewidth. The frequency of each laser beam is shifted by using acousto-optic modulators (AOM). The frequency of the dye laser is locked to the transfer cavity, which is a 50cm-length confocal cavity whose spacer is made of invar, a nickel steel alloy with low thermal expansion. Furthermore the transfer cavity is locked to the 556 nm laser light whose frequency is highly stabilized for laser cooling of Yb atoms as described below. The powers of MOT beam and MOT repumping beam are 11 mW and 12 mW, respectively and each of these beams is divided into three beams with a diameter of 10 mm, which produce the average peak intensities of each MOT beam and MOT repumping beam of  $1.4 I_s$  and  $1.6 I_s$ , respectively where  $I_s$  is the saturation intensity of the  $D_2$  line,

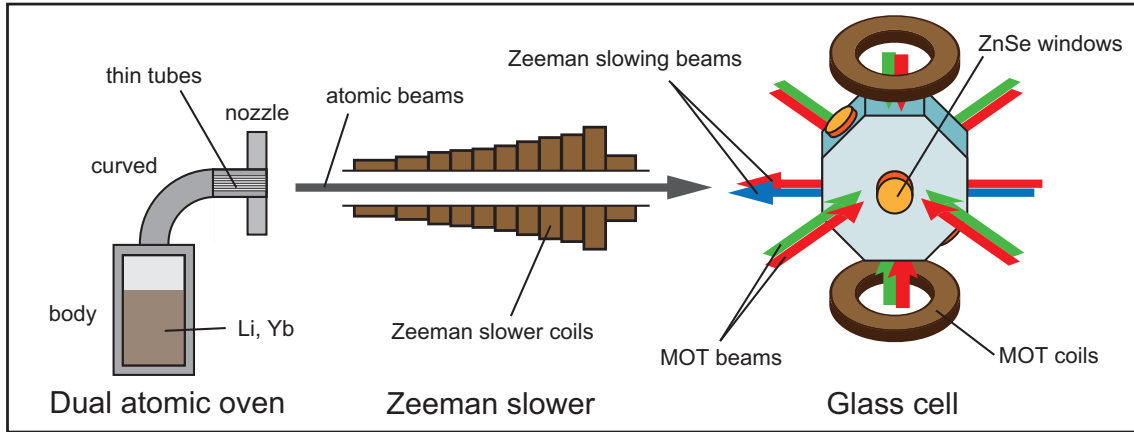


**Fig. 1** Schematic setup of the experiment. The Li and Yb metals are put in the dual atomic oven. Li and Yb atomic beams from the dual atomic oven are decelerated through the Zeeman slower coils by applying Zeeman slowing beams. These atoms are loaded to a MOT in the glass cell with ZnSe windows. MOT beams propagate along the three axes and the MOT coils are set in the vertical axis.

2.54 mW/cm<sup>2</sup>. The power of Zeeman slowing beam is 60 mW. MOT repumping beam is also used as probe repumping beam and the frequencies of the probe beam and probe repumping beam are set to the resonances of the transitions.

We use the transitions of  $^1S_0-^1P_1$  and  $^1S_0-^3P_1$  for laser cooling and probing of  $^{174}\text{Yb}$  atoms. Zeeman slowing of the atomic beam is done by using the strongly allowed  $^1S_0-^1P_1$  singlet transition, whose wavelength and natural linewidth are 399 nm and  $2\pi \times 29$  MHz, respectively. The LD chip is installed to the ECLD in the Littrow configuration and the wavelength is tuned to 798 nm by grating feedback. The output beam of the ECLD with a power of 10 mW is amplified to 480 mW by the TA with the operating current of 1.5 A. To convert the amplified laser light to 399 nm light, we used a periodically poled potassium titanyl phosphate (PPKTP) nonlinear crystal. The PPKTP crystal is put in a crystal oven made of copper whose temperature is stabilized by the Peltier unit. This crystal oven is set in a ring cavity to enhance the efficiency of second harmonic generation (SHG) and 399nm laser beam with a power of 40 mW is generated. The frequency of the 798 nm ECLD is locked to the transfer cavity and shifted by using the AOM.

Probing of  $^{174}\text{Yb}$  atoms is also done by using the  $^1S_0-^1P_1$  transition. Because we need a frequency stable laser light with good transverse mode to properly probe atoms, we adopted an ECLD with optical feedback to a filter cavity [16]. The ECLD is constructed in the Littrow configuration and the wavelength and the standard output power of the LD chip (NICHIA) are 399nm and 65 mW, respectively. The output beam of the ECLD with a power of 4.5 mW is injected to the filter cavity and then partially retro-reflected ( $\approx 4\%$ ) by a wedge plate to stabilize the laser frequency by optical feedback. In addition long-term stability of the frequency of the laser is obtained by 1f-3f electric feedback with modulation

frequency ( $f$ ) of 40 kHz. The output beam in  $\text{TEM}_{00}$  mode is obtained with a power of 2.1 mW. To lock the frequency of this laser system, we constructed a vacuum chamber with an atomic oven of Yb. The frequency stabilized output beam of the filter cavity is partially divided and applied to the atomic beam from the atomic oven, which contains 50 g of the natural Yb metals. The fluorescences from the atomic beam of Yb are detected by the PMT and the frequency of the laser system is locked to the resonance of  $^{174}\text{Yb}$ .

MOT of  $^{174}\text{Yb}$  atoms is done by using the intercombination  $^1S_0-^3P_1$  transition [17], whose wavelength and natural linewidth are 556 nm and  $2\pi \times 182$  kHz, respectively. The natural linewidth is so narrow that we use the high power narrow linewidth laser with a wavelength of 556 nm [18] as a light source. This laser system consists of a commercial 1 W fiber laser and a lithium triborate (LBO) nonlinear crystal in a ring cavity for SHG. The ytterbium-doped fiber laser with a wavelength of 1112 nm is frequency locked to a ultra-low-expansion (ULE) cavity mounted in a temperature-controlled vacuum chamber. This laser system generates 556 nm laser light with a linewidth of less than 100 kHz. The transfer cavity is locked to this frequency stabilized 556 nm laser light as described above. The power of MOT beam is 75 mW and divided into three beams with a diameter of 16 mm. This means that the average peak intensity of each MOT beam is about  $90 I_s$  where  $I_s$  is the saturated intensity of the  $^1S_0-^3P_1$  transition, 0.14 mW/cm<sup>2</sup>.

### 3.2 Glass cell

A main experimental region needs some conditions. It needs good optical accessibility for many laser beams used for laser cooling and probing of both atoms. It also needs to be compact because MOT and Feshbach coils put closer to the center of the main chamber can yield

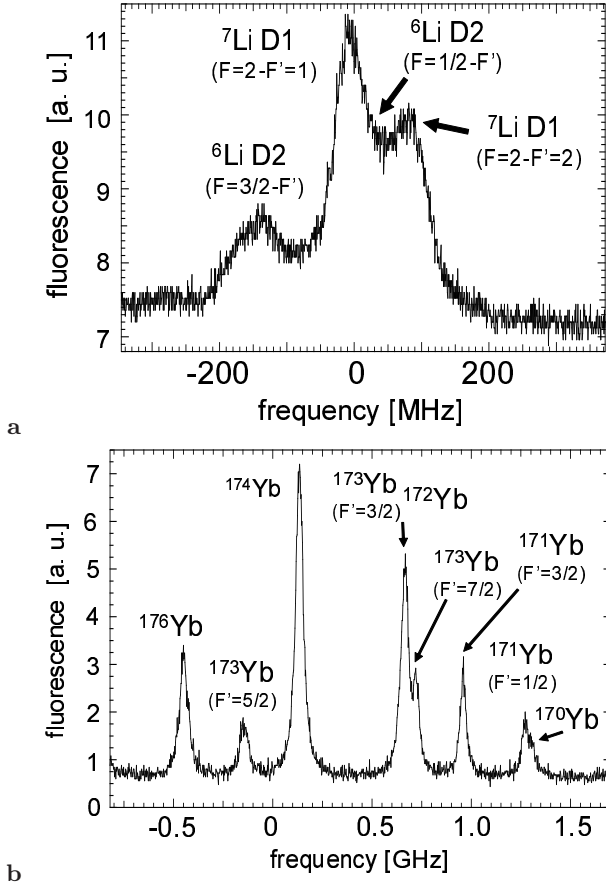


**Fig. 2** The fluorescence signals of the atomic beam of Li(a) and Yb(b). The Li and Yb metals with natural abundances were used in this measurement. Transitions of the  $D_2$  line of  $^6\text{Li}$  and the  $D_1$  line of  $^7\text{Li}$  ( $\lambda = 671$  nm) are observed (16 times integration)(a) and  $(6s^2) \ ^1S_0$ - $(6s6p) \ ^1P_1$  transitions of Yb isotopes ( $\lambda = 399$  nm) are observed(b). Each peak of signals is indicated by an isotope and a transition and  $F$  and  $F'$  denote hyperfine states of the ground state ( $S$ ) and the excited state ( $P$ ), respectively.

larger magnetic fields. To meet these conditions, we designed a octagonal glass cell made of TEMPAX Float (SCHOTT) as the main chamber as shown in the right side of Fig. 1. The pressure in the glass cell is estimated to be an order of  $10^{-9}$  Torr.

As light sources for optical trapping we chose the  $\text{CO}_2$  lasers with a wavelength of  $10.6 \mu\text{m}$ . The  $\text{CO}_2$  lasers have significantly longer wavelength than atomic transitions of Li and Yb, therefore electric fields of the  $\text{CO}_2$  laser beams are considered to be quasi-static electric field. This means that the  $\text{CO}_2$  lasers are useful for trapping Li and Yb atoms as well as LiYb molecules. For the  $\text{CO}_2$  laser beams, we attached four windows made of ZnSe that are AR coated at  $10.6 \mu\text{m}$  by using the adhesion bond (Epoxy technology, EPO-TEK 353ND) compatible with the ultra high vacuum.

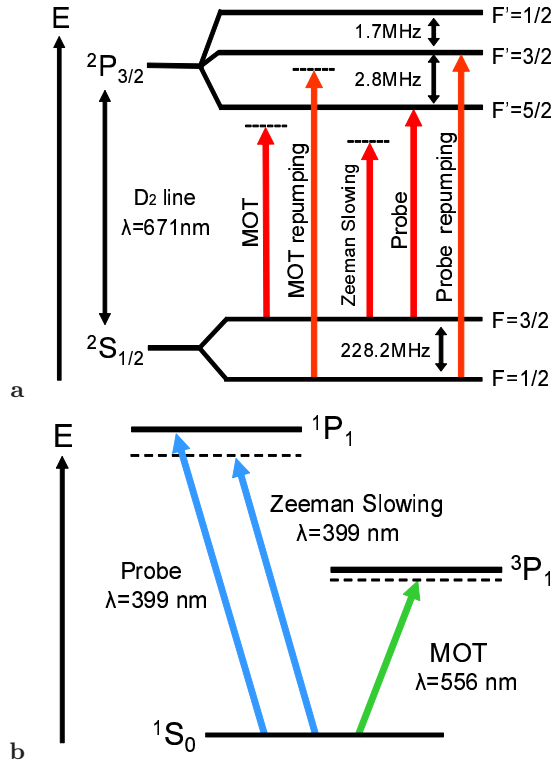


**Fig. 3** Energy levels and transitions for laser cooling and probing of  $^6\text{Li}$  (a) and  $^{174}\text{Yb}$  (b) atoms.

#### 4 Simultaneous magneto-optical trapping of Li and Yb atoms

In the experiment, more than 95%  $^6\text{Li}$  enriched Li metals and the natural Yb metals are put in the dual atomic oven, whose body part is heated to  $400^\circ\text{C}$ . Li and Yb atomic beams from the dual atomic oven are decelerated through the Zeeman slower coils by applying Zeeman slower beams of Li and Yb atoms as shown in the middle of Fig. 1. The Zeeman slower coils are in a increasing magnetic field configuration along the atomic beams and the maximum value of the magnetic field is designed approximately 520 G. Both Zeeman slowing beams are gradually focused towards the nozzle part of the dual atomic oven in accordance with the angular divergence of the atomic beams. The Zeeman slowed Li and Yb atoms are then loaded to a MOT in the glass cell. MOT beams propagate along the three axes and the MOT coils (anti-Helmholtz coils) are set in the vertical axis as shown in the right side of Fig. 1. The axial (radial) magnetic field gradients for the MOT are 16 G/cm (8 G/cm). The detunings of MOT beam, MOT repumping beam of Li and MOT beams of Yb are 24 MHz, 24 MHz ( $\sim 4.1 \Gamma$ ) and 4 MHz ( $\sim 22 \Gamma$ ), respectively. Zeeman slowing and MOT beams of Li and Yb atoms are overlapped at dichroic mirrors and then go through quarter wavelength plates designed for both wavelengths of laser beams in front of the glass cell. In these conditions,

we have successfully observed the fluorescences from the simultaneous MOT of  ${}^6\text{Li}$  and  ${}^{174}\text{Yb}$  atoms by a charge-coupled-device (CCD) camera. Loading of atoms to the simultaneous MOT is saturated within a few seconds, which is mainly limited by collisions of atoms with the background gases.

To increase the density and decrease the temperature of the atoms, we have implemented the compressed MOT for both atoms by increasing the magnetic field gradients and decreasing the detunings and the intensities of MOT beams. After the 2.5 s loading of atoms to the MOT, Zeeman slowing beams are shut off and the detunings of MOT beams, MOT repumping beams of Li and MOT beams of Yb are switched to 12 MHz, 12 MHz ( $\sim 2.0 I$ ) and 1 MHz ( $\sim 5.5 I$ ), respectively. Then the axial (radial) magnetic field gradients are linearly increased to 30 G/cm (15 G/cm) during a sweetening time of some tens of ms. After ramping the magnetic field gradients, the intensities of MOT beams of Li and Yb are decreased to approximately 1/10 and 1/20, respectively and the magnetic field gradients are kept at the maximum value during the cooling time. The atom number and the temperature of atoms in the compressed MOT are measured by the time-of-flight (TOF) method. The powers of probe beams of  ${}^6\text{Li}$  and  ${}^{174}\text{Yb}$  are 35  $\mu\text{W}$  and 50  $\mu\text{W}$ , respectively and the diameters of both probe beams are 6 mm. The density profiles of atoms right after turning off the MOT beams were obtained by absorption imaging technique as shown in Fig. 4. Typical values of the compressed MOT are as follows : The atom number ( $N$ ) and the temperature ( $T$ ) of the  ${}^6\text{Li}$  in the compressed MOT are  $N = 7 \times 10^3$  and  $T = 640 \mu\text{K}$ . Those values for  ${}^{174}\text{Yb}$  are  $N = 7 \times 10^4$  and  $T = 60 \mu\text{K}$ . These experimental parameters are listed in Table 1. Smaller number of Li atoms in the trap compared with Yb atoms is mainly originated from the fact that the configuration of the Zeeman slower was optimized for Yb atoms because the larger number of Yb atoms is necessary to sympathetically cool Li atoms through the collision between Li and Yb atoms in the optical trap. So far, we could not observe any additional disadvantage of simultaneous trapping on each atom number of Li and Yb in the MOT.

## 5 Conclusion

In summary, we have implemented the first simultaneous MOT of  ${}^6\text{Li}$  and  ${}^{174}\text{Yb}$  atoms. The dual atomic oven which contains both atomic species was developed and we have successfully observed the spectra of Li and Yb in the atomic beams from the dual atomic oven. Typical values of atom numbers and temperatures of the compressed MOT are  $7 \times 10^3$  atoms, 640  $\mu\text{K}$  for  ${}^6\text{Li}$ ,  $7 \times 10^4$  atoms and 60  $\mu\text{K}$  for  ${}^{174}\text{Yb}$ , respectively. The realization of the simultaneous MOT is the key to production of ultracold polar molecules of LiYb.

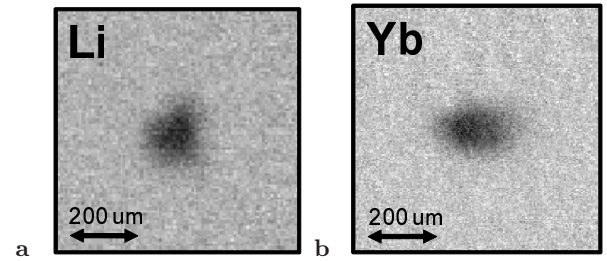


**Fig. 4** Absorption images of  ${}^6\text{Li}$  atoms(a) and  ${}^{174}\text{Yb}$  atoms(b) in the compressed MOT. These density profiles of atoms right after turning off the MOT beams were obtained by absorption imaging technique

**Table 1** Experimental parameters of the MOT of  ${}^6\text{Li}$  and  ${}^{174}\text{Yb}$ : Wavelength( $\lambda$ ) in vacuum, natural line width( $\Gamma$ ), saturation intensity( $I_s$ ), detunings( $\Delta$ ) of MOT beam (and MOT repumping beam of Li) and typical values of the atom number( $N$ ) and the temperature( $T$ ) of  ${}^6\text{Li}$  and  ${}^{174}\text{Yb}$  atoms in the compressed MOT.

|                             | ${}^6\text{Li}$ | ${}^{174}\text{Yb}$ |
|-----------------------------|-----------------|---------------------|
|                             | MOT             | repumping MOT       |
| $\lambda$ (nm)              | 670.977         | 555.8               |
| $\Gamma/2\pi$ (MHz)         | 5.9             | 0.182               |
| $I_s$ (mW/cm <sup>2</sup> ) | 2.54            | 0.14                |
| $I/I_s$                     | 1.4             | 1.6                 |
| $\Delta/\Gamma$             | 4.1             | 4.1                 |
| $N$                         | $7 \times 10^3$ | $7 \times 10^4$     |
| $T$ ( $\mu\text{K}$ )       | 640             | 60                  |

The improvement of the vacuum of the main chamber will reduce the atom losses of the MOT due to the background gases and this will increase the atom number of the simultaneous MOT. In addition to this improvement, further optimization of the compressed MOT are expected to decrease temperatures of the compressed MOT closer to the Doppler cooling limits of  ${}^6\text{Li}$  and  ${}^{174}\text{Yb}$ ,  $T = 140 \mu\text{K}$  and  $T = 4 \mu\text{K}$ , respectively. These improvements will increase the phase space density of the simultaneous MOT and this leads to the next process, optical trapping by  $\text{CO}_2$  lasers. We can examine the collisional properties of Li and Yb in the optical trap and obtain the information for production of LiYb molecules.

*Acknowledgements* We thank H. Sadeghpour, P. Zhang, G. Gopakumar, and M. Abe for helpful discussions and acknowledge K. Hayasaka, H. Ohira, K. Uchida, and S. Yabunaka for experimental assistance. This work was partially supported by Grant-in-Aid for Scientific Research of JSPS (No. 18204035) and the Global COE program "The Next Generation of Physics, Spun from Universality and Emergence" from the Ministry of Education, Culture, Sports, Science and Technology (MEXT) of Japan. M. O. acknowledges support from JSPS.

## References

1. M. H. Anderson, J. R. Ensher, M. R. Matthews, C. E. Wieman, E. A. Cornell, *Science* **269**, 198 (1995)
2. K. B. Davis, M.-O. Mewes, M. R. Andrews, N. J. van Druten, D. S. Durfee, D. M. Kurn, W. Ketterle, *Phys. Rev. Lett.* **75**, 3969 (1995)
3. B. DeMarco, D. S. Jin, *Science* **285**, 1703 (1999)
4. J. Doyle, B. Friedrich, R. V. Krems, F. Masnou-Seeuws, *Eur. Phys. J. D* **31**, 149 (2004)
5. R. V. Krems, B. Friedrich, W. C. Stwalley, *Cold Molecules: Theory, Experiment, Applications* (CRC Press, Boca Raton, FL, 2009)
6. D. DeMille, *Phys. Rev. Lett.* **88**, 067901 (2002)
7. M. Lewenstein, *Nature Phys.* **2**, 309 (2006)
8. A. Micheli, G. K. Brennen, P. Zoller, *Nature Phys.* **2**, 341 (2006)
9. M. Okano, H. Hara, Y. Takasu, Y. Takahashi, The 21st Century COE Symp. **48**, Kyoto Univ. Clock Tower Centennial Hall (2007)
10. N. Nemitz, F. Baumer, F. Münchow, S. Tassy, A. Görlitz, *Phys. Rev. A* **79**, 061403(R) (2009)
11. B. Marcelis, S. J. J. M. F. Kokkelmans, G. V. Shlyapnikov, D. S. Petrov, *Phys. Rev. A* **77**, 032707 (2008)
12. G. Modugno, G. Ferrari, G. Roati, R. J. Brecha, A. Simoni, M. Inguscio, *Science* **294**, 1320 (2001)
13. T. Köhler, K. Góral, P. S. Julienne, *Rev. Mod. Phys.* **78**, 1311 (2006)
14. K.-K. Ni, S. Ospelkaus, M. H. G. de Miranda, A. Pe'er, B. Neyenhuis, J. J. Zirbel, S. Kotochigova, P. S. Julienne, D. S. Jin, J. Ye, *Science* **322**, 231 (2008)
15. L. Windholz, M. Musso, G. Zerza, H. Jäger, *Phys. Rev. A* **46**, 5812 (1992)
16. J. Labaziewicz, P. Richerme, K. R. Brown, I. L. Chuang, K. Hayasaka, *Opt. Lett.* **32**, 572 (2007)
17. T. Kuwamoto, K. Honda, Y. Takahashi, T. Yabuzaki, *Phys. Rev. A* **60**, R745 (1999)
18. S. Uetake, A. Yamaguchi, S. Kato, Y. Takahashi, *Appl. Phys. B* **92**, 33 (2008)